Scripta Materialia 180 (2020) 88–92

Contents lists available at ScienceDirect

Scripta Materialia

journal homepage: www.elsevier.com/locate/scriptamat

Mechanism of Sc poisoning of Al-5Ti-1B grain refiner

Jinxian Huang[a], Lei Feng[a], Cong Li[b,*], Chunfa Huang[a], Jianguo Li[a,*], Bernd Friedrich[b]

[a] School of Materials Science and Engineering, Tsinghua University, 100084 Beijing, China
[b] IME Institute of Process Metallurgy and Metal Recycling, RWTH Aachen University, 52056 Aachen, Germany

ARTICLE INFO

Article history:
Received 10 December 2019
Revised 26 January 2020
Accepted 27 January 2020

Keywords:
Poisoning
Grain refinement
Scandium
Geometric phase analysis

ABSTRACT

A poisoning effect of scandium (Sc) with respect to Al-5Ti-1B (in wt.%) grain refiner was investigated for the first time. Grain refinement effect of Al-5Ti-1B was found to fade in Al alloys with content of trace Sc. The modification of TiB_2 particle by inward diffusion of Sc was characterized by high-resolution transmission electron microscope (HRTEM). Through Geometric Phase Analysis (GPA) analysis, a notable increase of stress concentration at (0001) plane of Sc-modified TiB_2 was revealed, the result of which shed lights on the mechanism of Sc poisoning effect.

© 2020 Acta Materialia Inc. Published by Elsevier Ltd. All rights reserved.

Grain refinement is an efficient way to improve mechanical properties of alloys. Through chemical inoculation of grain refiner (e.g., Al-5Ti-1B), fine and equiaxed grain structures can be achieved. In aluminum alloys, several series of Al-Ti-B master alloys have been developed as grain refiners, among which Al-5Ti-1B is the most widely used one [1]. So far, several theories have been proposed in order to clarify mechanism of grain refinement [2–6]. Substantial amount of researches demonstrated that TiB_2 particles inoculated into Al melt via Al-Ti-B master alloys enhanced heterogeneous nucleation of α-Al grains and solute Ti atoms promoted the nucleation efficiency of TiB_2 until a complete wetting of TiB_2 particles by solid aluminum [7–9].

Zr, Cr, Sc are important trace alloying elements in aluminum alloys. The addition of those elements improves mechanical properties of the alloy through precipitation strengthening [10]. Meanwhile, these elements are also known as effective grain refiners despite their effects are not as remarkable as that of Al-Ti-B master alloys.

However, the presence of some solute elements (e.g., Zr, Cr) is not always beneficial for Al alloys, especially when the alloys are planned to be treated with grain refiners. It has been reported that when Al alloys contained Zr, Cr or excess Si, the refining performance of Al-Ti-B grain refiners dramatically faded [11,12]. This adverse effect of Zr, Cr or excess Si on Al-Ti-B grain refiners is generally termed as “poisoning effect”. The explanation lies primarily in the interaction between certain solute elements e.g., Zr and TiB_2 particles. It was reported in detail by Fan et al. [11] that at the presence of Zr, an atomic monolayer Ti_2Zr was formed upon the (0001) surface of TiB_2. Such a layer destroyed the otherwise intact Ti-terminated interface, which was believed to be essential for heterogeneous nucleation of α-Al. In another early publication, Sc was mentioned to have solid solubility in the layer of titanium aluminide (Al_3Ti), which indicated the potential of Sc being a poisoning element for TiB_2 [13]. A recent work offered another clue in understanding poising effect. Jing et al. [14] reported that addition of certain alloying elements, e.g., Cu, Si into aluminum affected the lattice parameter of α-Al. For certain inoculated particles e.g. LaB_6, the potential of them acting as nucleation cites will be deteriorated due to an increased lattice misfit between LaB_6 and α-Al.

To the best of our knowledge, the poisoning effect of Sc on Al-Ti-B grain refiners has not been experimentally studied in detail. In the present study, the poisoning effect of Sc was investigated and the mechanism behind was discussed based on microstructural characterization of Sc-modified TiB_2 particles.

Commercial pure aluminum (99.7 wt.% Al, CP-Al), Al-4Mg alloy (4 wt.% Mg) and Al-5Ti-1B master alloy were used as the raw materials for experiments. Al-4Mg alloy was selected in addition to CP-Al alloy in order to verify the poisoning effect of Sc in different Al alloy systems. Meanwhile, Al-Mg is an important alloy series where Sc is sometimes added intentionally [15,16]. For each experiment, 1.5 kg of CP-Al was melted to 760 °C and set rest for 30 min in a clay-graphite crucible placed inside a resistance furnace. Desired *Sc* content of the alloys was realized by charging Al-2Sc master alloy. The standard TP-1 test was conducted so as to assess the efficiency of grain refinement [17]. In certain trials, Al-5Ti-1B was added into the alloyed melt at 760 °C. The melt with and

* Corresponding authors.
E-mail addresses: cli@ime-aachen.de (C. Li), jg.li@mail.tsinghua.edu.cn (J. Li).

https://doi.org/10.1016/j.scriptamat.2020.01.031
1359-6462/© 2020 Acta Materialia Inc. Published by Elsevier Ltd. All rights reserved.

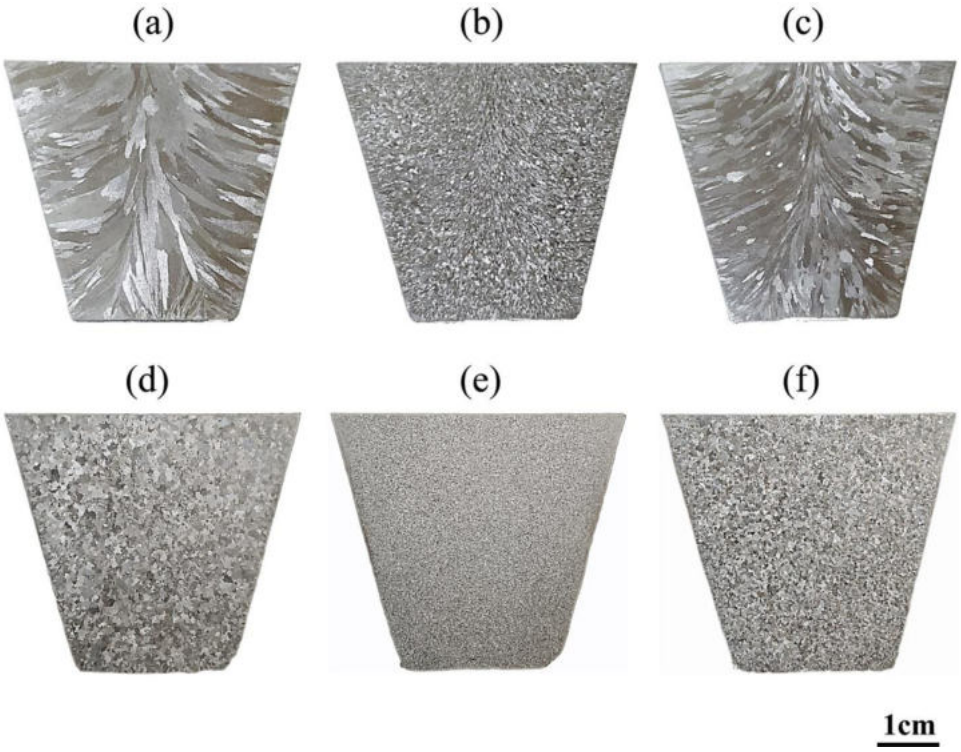

Fig. 1. Macrographs show the grain structure on longitudinal section of TP-1 samples: (a)(d) as-cast; (b)(e) addition of 0.2 wt.% Al-5Ti-1B grain refiner; (c)(f) addition of 0.2 wt.% Al-5T-1B and 0.1 wt.% Sc. (a)–(c) for CP-Al, and (d)–(f) for Al-4Mg alloy.

without addition of Al-5Ti-1B was poured at 720 °C into a 350 °C TP-1 mold cooled by a 3.8 L/min water flow.

The samples used for grain refinement assessment were sectioned longitudinally from 38 mm height from the bottom to the top of the TP-1 ingot. The samples were polished and corroded according to standard metallographic techniques. The grain structure of samples was examined via an optical microscope with polarized light after anodized in Barker's reagent. The grain size was measured by the linear intercept method. The sample used for microstructural characterization were electrochemically polished and analyzed via a HITACHI SU8220 cold field emission scanning electron microscope (SEM). The sample used for high-resolution transmission electron microscope (HRTEM) analysis was prepared through the focused ion beam (FIB). The HRTEM analysis was conducted using a FEI Tecnai G2 transmission electron microscope (TEM) operating at an acceleration voltage of 300 kV.

Fig. 1 presents the macrostructure of samples. The as-cast CP-Al shows a completely coarse columnar grain structure with an averaged grain size of 1233 μm (Fig. 1(a)). As Fig. 1(b) shows, introduction of 0.2 wt.% Al-5Ti-1B resulted in an expected equiaxed and fine grain structure with grain size of 291 μm. The presence of 0.1 wt.% Sc adversely affected the grain refinement efficiency of Al-5Ti-1B, as was evidenced from coarse columnar grain structure and a corresponding grain size of 914 μm (Fig. 1(c)). For Al-4Mg alloy samples, the grain size of Al-4Mg alloy without and with grain refiner was 572 μm and 147 μm, respectively, as shown in Fig. 1(d) and (e). When *Sc* was introduced into the Al-4Mg alloy, addition of Al-5Ti-1B only led to limitedly reduced grain size of 471 μm (Fig. 1(f)). Fig. 1(a)–(f) clearly demonstrate the poisoning effect of Sc, i.e., the presence of Sc offset grain refinement effect of Al-5Ti-1B. Furthermore, the poisoning effect of Sc applies not only to CP-Al but also to Al-Mg binary alloy.

Over the remainder part of the article, the observed Sc poisoning phenomena was elucidated, using as an example, the sample prepared by adding Al-5Ti-B grain refiner into Sc-bearing CP-Al (Fig. 1(b)). Fig. 2 presents the microstructure as well as EDS mapping result of a cluster composed of TiB_2 particles and Al_xFe intermetallic which was regularly observed on the polished surface. It was observed that the distribution of Sc corresponded well with that of Ti and B, which suggested a probable incorporation of Sc into TiB_2 particles. Fe element was detected at discrete regions of the mapping area where Ti and B signal faded. Such an observation demonstrated the agglomeration of Sc-modified TiB_2 particles and Al_xFe intermetallic at local area of the sample after solidification. As Al_xFe intermetallic is known as a secondary intermetallic precipitating at the grain boundary of CP-Al, it is believed that during solidification, a large portion of Sc-modified TiB_2 particles was pushed towards the grain boundary region where they agglomerated either internally or externally with Al_xFe intermetallic. As a corollary, those Sc-modified TiB_2 particles failed to contribute to grain refinement.

HRTEM were employed to gain insights into the interaction between TiB_2 particle and Sc. The used specimen was from CP-Al with addition of 0.2 wt.% Al-5Ti-1B and 0.1 wt.% Sc. FIB was employed in order to prepare a milled slice from the grain boundary where TiB_2 and Al_xFe agglomerated. The specimen was characterized by TEM and EDS line scan. The corresponding results are shown in Fig. 3. It can be seen that TiB_2 particle cohered with an Al_xFe intermetallic. Sc was found to vary in an equivalent tendency with Ti and B, which validated the modification of TiB_2 particles by inward diffusion of Sc. Such a feature differed from the reported modification of TiB_2 particles by surface segregation of Zr [11]. For TiB_2 particles inoculated into Al melt at absence of Sc, the (0001) surface of TiB_2 contains Ti-terminated and B-terminated interface, the latter of which is more stable due to lower surface energy. Similar to TiB_2, ScB_2 has a HCP crystal structure (space group P6/mmm) and Sc- and B- terminated interface at (0001) surface [18]. However, the Sc-terminated interface is more stable than the B-terminated interface. Given at the same time the greater chemical potential and diffusivity coefficient of Sc than Ti

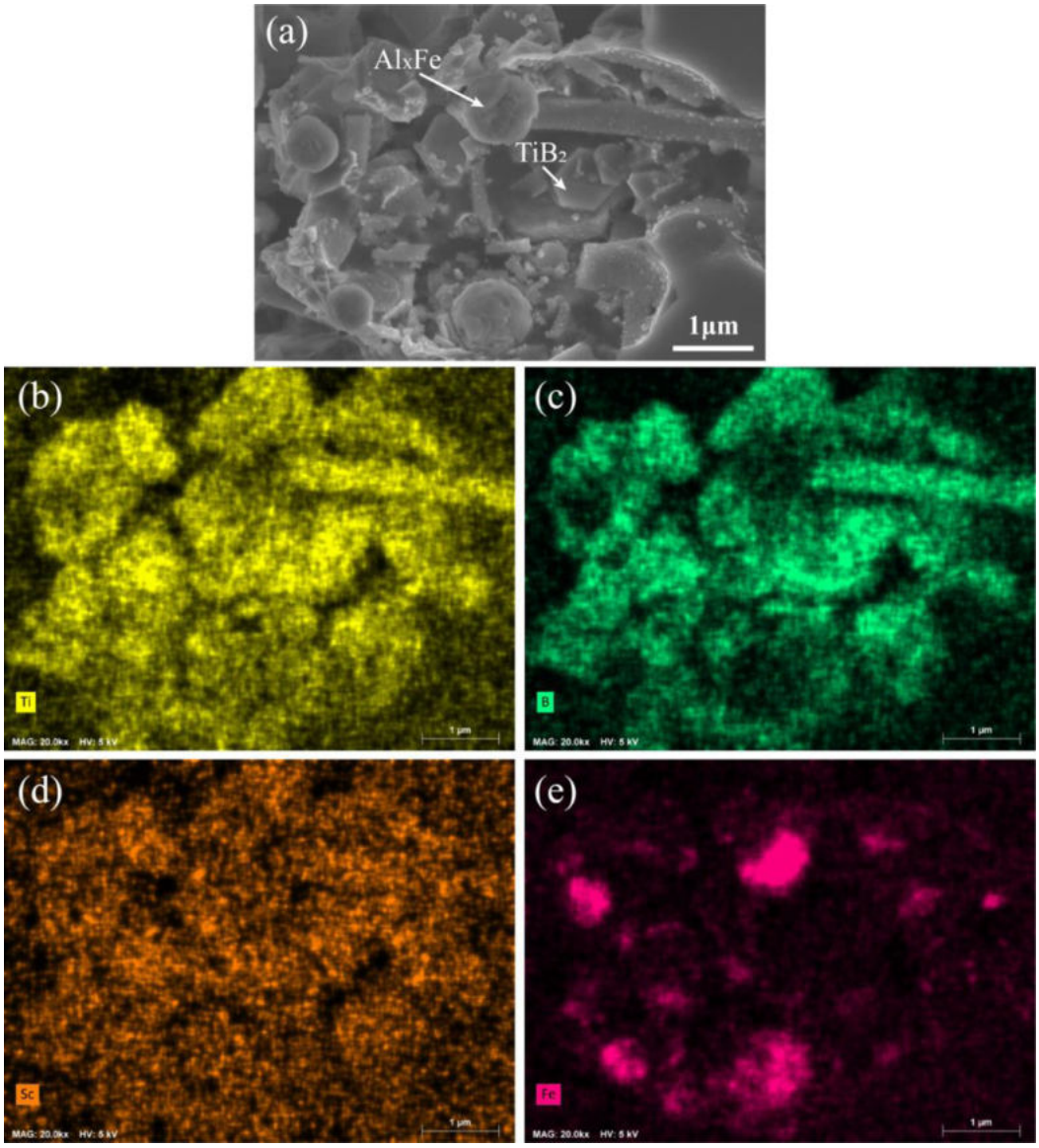

Fig. 2. (a) SEM image of a cluster composed of TiB_2 particles and Al_xFe, the sample is from CP-Al with addition of 0.2 wt.% Al-5T-1B and 0.1 wt.% Sc; (b–e) EDS elemental mapping with respects to (b) Ti, (c) B, (d) Sc and (e) Fe.

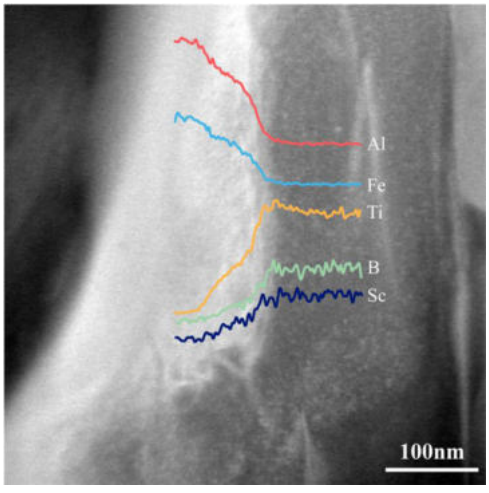

Fig. 3. TEM micrograph shows a platelet TiB_2 particle cohering with Al_xFe with imposition of the result of elemental line scan.

($D_{Sc}/D_{Ti} = 3.3 \times 10^5$ [19]), it is proposed that the diffusion of Sc into TiB_2 was realized by substitution of Ti by Sc. And as a result, a (Ti, Sc)B_2 phase will be formed.

EDS line scan result shows that both Fe and Al signal vary continuously at the interface between TiB_2 and Al_xFe, which indicated a possible heterogeneous nucleation of Al_xFe intermetallic upon Sc-modified TiB_2. Such a nucleation can partially explain the inter-particle agglomeration between TiB_2 particles and Al_xFe intermetallic.

Geometric phase analysis (GPA) method, a helpful tool for quantitatively measuring the strain field based on the HRTEM image, was used to elucidate the poisoning effect of Sc from thermodynamic point of view. By measuring the displacement of lattice fringes of HRTEM image with respect to a reference unstrained area, the local Fourier components of lattice fringes is calculated so that the information concerning the strain of lattice can be extracted by analyzing interference fringes [20]. The GPA method is based upon centering an aperture around the assigned reflection in the Fourier Transformation of an HRTEM image and subsequently performing an inverse Fourier Transformation. The phase of image,

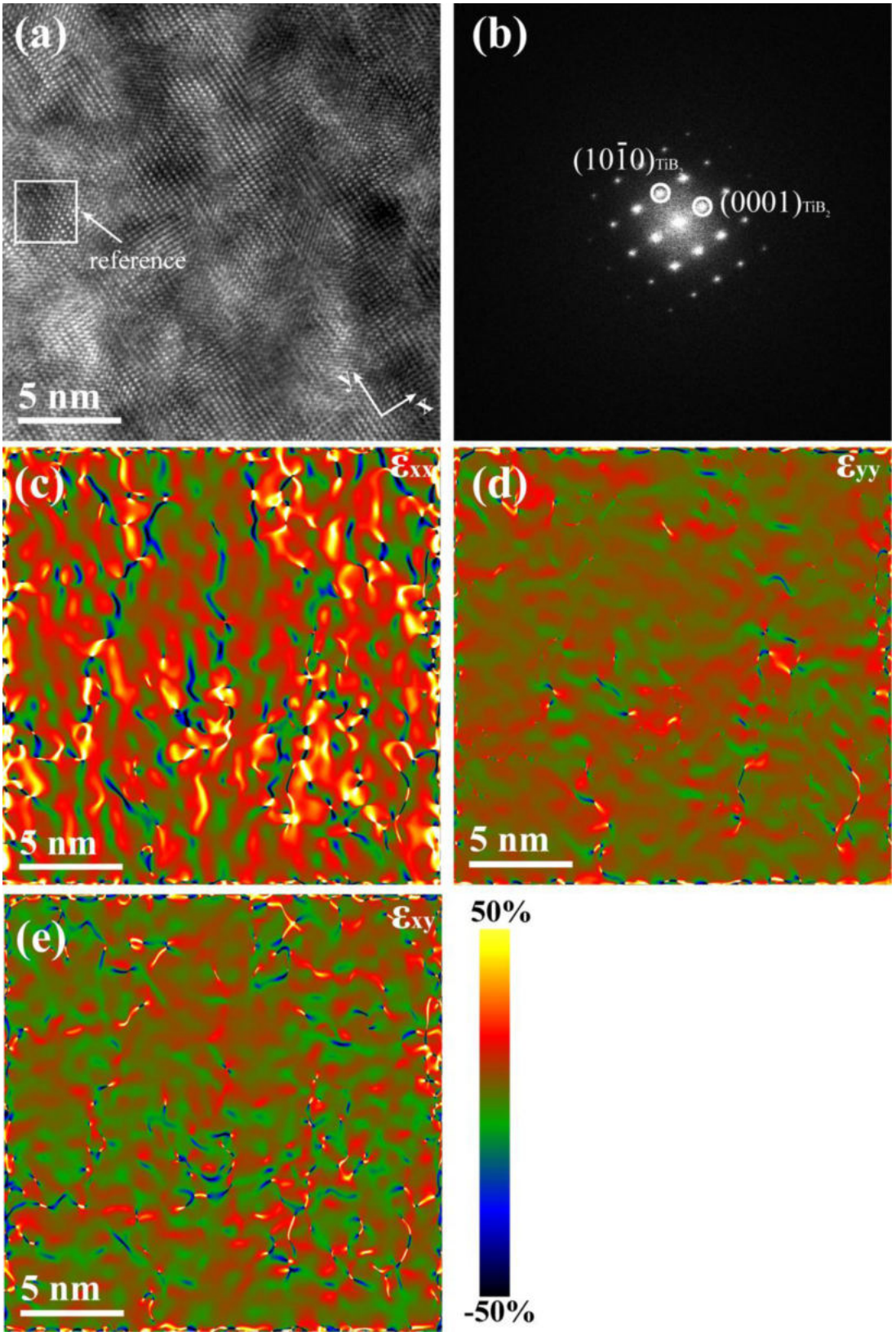

Fig. 4. (a) HRTEM lattice image of TiB_2 along [010] direction, the white square shows the reference region; (b) power spectrum of the HRTEM image and the analyzed spots; (c)-(e) the strain fields of ε_{xx}, ε_{yy}, ε_{xy}, respectively.

namely geometric phase $\boldsymbol{P_g(r)}$, related to the component of displacement field $\boldsymbol{u(r)}$ in the direction of the reciprocal lattice vector, $\boldsymbol{g}$ [21]:

$$\boldsymbol{P}_{\mathrm{g}}(r) = -2\pi \boldsymbol{g} \cdot \boldsymbol{u}(r) \tag{1}$$

where $\mathbf{r}$ is the position in the image. A two-dimensional lattice is defined in real space basis vectors, $\mathbf{a_1}$ and $\mathbf{a_2}$ which correspond to the reciprocal lattice vectors $\mathbf{g_1}$ and $\mathbf{g_2}$. Through calculating two sets of lattice fringes, the displacement field is given by [20]:

$$\boldsymbol{u}(r) = -\frac{1}{2\pi}\left[\boldsymbol{P_{g1}}(r)\boldsymbol{a}_1 + \boldsymbol{P}_{\mathrm{g2}}(r)\boldsymbol{a}_2\right] \tag{2}$$

The information of local strain can be obtained by analyzing the gradient of the displacement field, which is defined as $\boldsymbol{\varepsilon}$ and described as follows:

$$\varepsilon = \begin{pmatrix} \varepsilon_{xx} & \varepsilon_{xy} \\ \varepsilon_{yx} & \varepsilon_{yy} \end{pmatrix} = \begin{pmatrix} \frac{\partial u_x}{\partial x} & \frac{\partial u_x}{\partial y} \\ \frac{\partial u_y}{\partial x} & \frac{\partial u_y}{\partial y} \end{pmatrix} \tag{3}$$

In the above matrix, the value of each element can be converted to an image. More details about GPA method can be found in Hÿtch's work [20].

In the current work, GPA was conducted in Digital Micrograph by FRWR plugin. GPA maps used for the investigation of elastic strain within TiB_2 particle are shown in Fig. 4 where strain changes ranging from −50% to +50% are reflected by different color scale. The reference region without strain is shown in Fig. 4(a), featured by the distinct and undistorted fringes. In order to obtain results with the best signal-to-noise ratio, two non-collinear reciprocal lattice vectors as well as the most intense spots in the power spectrum (Fig. 4(b)) were chosen for analysis with *x*-axis coincide with the (0001) direction and the *y*-axis with the $(10\bar{1}0)$ direction of the lattice, as is shown in Fig. 4(b). For Sc-modified TiB_2, strain concentration was identified in either x-, y- or xy-component of the strain field, suggesting an increased interfacial energy. In the strain field of $\boldsymbol{\varepsilon_{xx}}$ (Fig. 4(c)), there are quite a few convergence regions of strain with relatively high strain intensity. The strain condition of $\boldsymbol{\varepsilon_{yy}}$ and $\boldsymbol{\varepsilon_{xy}}$ with respect to amount of strain convergence regions and the strain intensity (Fig. 4(d)-(e)) was however much less than that of $\boldsymbol{\varepsilon_{xx}}$, which suggested a primary strain concentration in strain field $\boldsymbol{\varepsilon_{xx}}$ of TiB_2 at the presence of Sc. And $\boldsymbol{\varepsilon_{xx}}$ stands for (0001) plane of TiB_2. Such strain concentration at (0001) plane can be explained by formation of (Ti,Sc)B_2 at the presence of Sc. On account of a bigger atom radius of Sc, (Ti, Sc)B_2 has a greater lattice parameter than TiB_2, especially upon the (0001) surface. As (0001) plane is also the hexagonal platelets of TiB_2 where heterogeneous nucleation of α-Al takes place [6,22], a strain concentration on this plane will remarkably deteriorated the potential of TiB_2 acting as heterogeneous nuclei.

In conclusion, the poisoning effect of Sc with respect to Al-5Ti-1B in CP-Al and Al-Mg system was investigated for the first time. TiB_2 particles were modified by inward diffusion of Sc. Such Sc-modified TiB_2 particles failed to contribute to grain refinement and were pushed towards the grain boundaries where they agglomerated and acted as nucleation substrate for Al_xFe intermetallic. According to GPA analysis, poisoning effect of Sc can be explained by strain concentration at (0001) plane of Sc-modified TiB_2. Result of the present work implies that more cautions should be paid in choosing grain refiner for Sc-containing Al alloys.

Declaration of Competing Interest

The authors declare that they have no known competing financial interests or personal relationships that could have appeared to influence the work reported in this paper.

Acknowledgements

This work was supported by Tsinghua University Initiative Scientific Research Program (Grant No. 20173080030) and the International Science and Technology Cooperation Project of China (Grant No. 2015DFR50470).

References

[1] L. Zhou, F. Gao, G.S. Peng, N. Alba-Baena, J. Alloys Compd. 689 (2016) 401–407.
[2] Z. Fan, Metall. Mater. Trans. A Phys. Metall. Mater. Sci. 44 (2013) 1409–1418.
[3] I.G. Davies, J.M. Dennis, A. Hellawell, Metall. Trans. 1 (1970) 275–280.
[4] G.P. Jones, J. Pearson, Metall. Trans. B 7 (1976) 223–234.
[5] M. Johnsson, L. Backerud, G.K. Sigworth, Metall. Trans. A 24 (1993) 481–491.
[6] A.L. Greer, J. Chem. Phys. 145 (2016) 211704.
[7] L. Zhang, Q. Zheng, H. Jiang, J. Zhao, Scr. Mater. 160 (2019) 25–28.
[8] B.S. Murty, S.A. Kori, M. Chakraborty, Int. Mater. Rev. 47 (2002) 3–29.
[9] Z. Fan, Y. Wang, Y. Zhang, T. Qin, X.R. Zhou, G.E. Thompson, T. Pennycook, T. Hashimoto, Acta Mater. 84 (2015) 292–304.
[10] S. Costa, H. Puga, J. Barbosa, A.M.P. Pinto, Mater. Des. 42 (2012) 347–352.
[11] Y. Wang, C.M. Fang, L. Zhou, T. Hashimoto, X. Zhou, Q.M. Ramasse, Z. Fan, Acta Mater. 164 (2019) 428–439.
[12] D. Qiu, J.A. Taylor, M.X. Zhang, P.M. Kelly, Acta Mater. 55 (2007) 1447–1456.
[13] B. Cantor, K. O'Reilly, Solidification and Casting, CRC Press, 2003.
[14] L. Jing, T. Lu, Y. Pan, Jom (2019) 1–8.
[15] J. Taendl, A. Orthacker, H. Amenitsch, G. Kothleitner, C. Poletti, Acta Mater. 117 (2016) 43–50.
[16] N. Kumar, R.S. Mishra, C.S. Huskamp, K.K. Sankaran, Scr. Mater. 64 (2011) 576–579.
[17] Z. Fan, F. Gao, L. Zhou, S.Z. Lu, Acta Mater. 152 (2018) 248–257.
[18] H. Zhao, N. Qin, Appl. Surf. Sci. 258 (2012) 3328–3330.
[19] M.E. Van Dalen, D.C. Dunand, D.N. Seidman, Acta Mater. 53 (2005) 4225–4235.
[20] M.J. Hÿtch, E. Snoeck, R. Kilaas, Ultramicroscopy 74 (1998) 131–146.
[21] Y. Wang, X.P. Liu, G.W. Qin, Mater. Charact. 106 (2015) 308–316.
[22] T.E. Quested, Mater. Sci. Technol. 20 (2004) 1357–1369.